A 24 keV liquid-metal-jet x-ray source for biomedical applications

D. H. Larsson,[a] P. A. C. Takman,[b] U. Lundström, A. Burvall, and H. M. Hertz
Biomedical and X-Ray Physics, Department of Applied Physics, Royal Institute of Technology/Albanova, SE-10691 Stockholm, Sweden

(Received 24 September 2011; accepted 7 November 2011; published online 1 December 2011)

We present a high-brightness 24-keV electron-impact microfocus x-ray source based on continuous operation of a heated liquid-indium/gallium-jet anode. The 30–70 W electron beam is magnetically focused onto the jet, producing a circular 7–13 μm full width half maximum x-ray spot. The measured spectral brightness at the 24.2 keV In K_α line is 3×10^9 photons/(s $\times$ mm^2 $\times$ mrad^2 $\times$ 0.1% BW) at 30 W electron-beam power. The high photon energy compared to existing liquid-metal-jet sources increases the penetration depth and allows imaging of thicker samples. The applicability of the source in the biomedical field is demonstrated by high-resolution imaging of a mammography phantom and a phase-contrast angiography phantom. © *2011 American Institute of Physics*. [doi:10.1063/1.3664870]

I. INTRODUCTION

Liquid-metal-jet anodes[1,2] show promise to take electron-impact x-ray microfocus sources to unprecedented brightness, thereby improving performance in a number of important applications from x-ray diffraction to phase-contrast imaging. However, present liquid-metal-jet source systems are typically optimized for around 10 keV line emission, whereas many applications, especially in the biomedical area, require higher energies in order to allow examination of thicker samples. Here we describe details of the high-brightness continuous operation of a 24 keV characteristic line emission microfocus source based on a heated liquid indium/gallium jet anode.

The x-ray brightness of electron-impact sources is proportional to the e-beam power density (kW/mm^2). The major limiting factor on increasing the power density is the thermal load capacity of the target, since ~99% of the kinetic energy of the electron beam is converted into heat.[3] Therefore, the stationary-anode arrangement classically used in few-tens-of-keV microfocus sources relies on high-melting-point metals such as Mo, W, or Ag. For microfocus x-ray sources with circular foci (typically less than a few tens of micrometers in diameter), the maximum e-beam power loading[4] is in the range 0.4–0.8 W per electron-beam diameter in micrometers (FWHM of Gaussian beam). This corresponds to an e-beam power density at the anode of 25–50 kW/mm^2 for a 20 μm source. High-end rotating-anode systems (e.g., FR-E+ SuperBright, Rigaku) can operate at similar e-beam power density with elongated 700 $\times$ 70 μm^2 spot sizes. For this geometry, angled viewing of the line focus produces a circular x-ray spot which increases the apparent, but not the actual, e-beam power density.

Liquid-metal-jet sources were first demonstrated with solder[1,5] and tin[6] anodes in batch-operated systems. Although these systems produced line emission around 25 keV (e.g., Sn K_α), the high melting point (T_m) of the anodes ($T_m = 183$°C for 63% Sn, 37% Pb) makes continuous operation nontrivial as it requires circulation of the liquid metal at uniform and elevated temperatures. The method was then extended to lower temperature anodes (Ga, $T_m = 30$°C) producing Ga K_α 9 keV line emission but still in batch operation.[2] The first successful system with continuous operation (JXS-D1, Excillum AB) is based on room-temperature liquid alloys such as Ga/In/Sn ($T_m = -19$°C). The emission spectrum is typically dominated by the 9.2 keV Ga line while the other elements contribute marginally. These systems can, e.g., be operated at 40 W with a circular 7 μm FWHM x-ray spot or at 200 W with angled viewing of an 80 $\times$ 20 μm^2 line focus. Such high-brightness 10 keV sources are suitable for, e.g., high-end scattering and diffraction studies[7,8] and phase-contrast imaging of thin objects.[9] However, many scattering applications (e.g., small-angle x-ray scattering, SAXS) require penetration of thicker samples and many potential phase-contrast imaging applications are for samples at least a few cm thick (small-animal studies, mammography, etc.). Consequently, high-brightness liquid-jet sources operating at higher energies and, thus, increasing the transmission could open up new areas of applications.

In the present paper, we demonstrate a high-brightness liquid-metal-jet microfocus source for continuous operation in the few-tens-of-keV regime. The source is based on a heated indium/gallium-anode. By increasing the In content, we increase the brightness of the 24 keV In K_α line emission. However, this is done at the expense of a higher operating temperature ($T_m = 70$°C). The source is typically operated at 40 W with a 7 $\times$ 7 μm^2 FWHM x-ray spot, corresponding to 5.7 W/μm and 1000 kW/mm^2, and the present power limitation is due to contamination of the electron-emitting cathode by metal vapor. Below, the source and its performance are described and characterized in detail. Furthermore, we demonstrate its capabilities for high-resolution phase- and absorption-contrast imaging of two thick objects, a mammography phantom and an angiography phantom.

[a]Author to whom correspondence should be addressed. Electronic mail: daniel.larsson@biox.kth.se.
[b]Present address: Excillum AB, Kista, Sweden.

 © 2011 American Institute of Physics

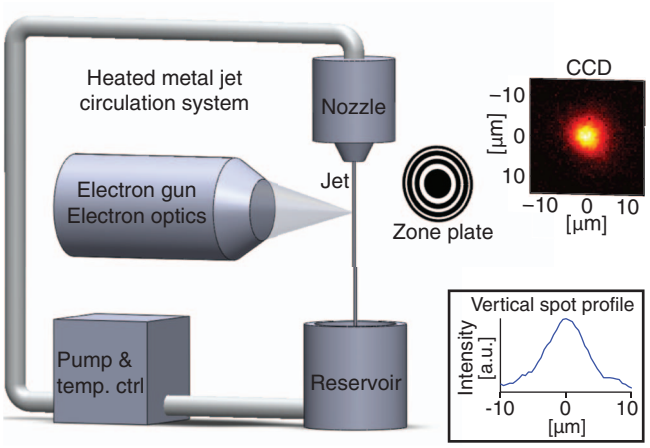

FIG. 1. (Color online) Experimental arrangement showing the heated In/Ga jet and the zone plate imaging arrangement. The measured x-ray spot distribution and vertical spot profile (inset) are also displayed.

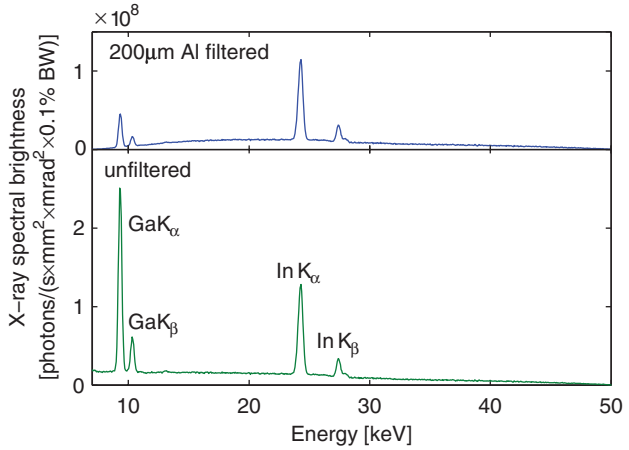

FIG. 2. (Color online) Calibrated emission spectrum recorded at 30 W with a 7 × 7 μm^2 x-ray spot. Lower curve: unfiltered spectrum. Upper curve: 200 μm thick Al hardened spectrum.

II. EXPERIMENTAL ARRANGEMENT

Figure 1 illustrates the experimental arrangement. It is based on the JXS-R5 source platform (Excillum AB) that has been modified to allow liquid-metal-jet operation at temperatures up to 100°C.

The source platform consists of several subsystems, such as vacuum pumps, a metal-jet circulation system, electron gun, and electron optics. In its original configuration it circulates a Ga/In/Sn alloy (68.5% Ga, 21.5% In, and 10% Sn), which is liquid at room temperature. In order to operate the system using a Ga/In alloy (35% Ga and 65% In), with a melting point of 70°C, heating of the liquid-metal circulation system is required. This has been accomplished by attaching a regulated water heater to the original water cooling system. As all parts of the circulation system are not effectively heated by the water heater, additional heating is provided by externally controlled heating tapes. To avoid cold spots that may cause freezing of the liquid metal, the heated parts of the system are insulated using standard water pipe insulation. A sapphire pinhole nozzle with a 150 μm orifice is used to form a regenerative jet using 180 bars of backing pressure supplied by the circulation system. The electron-beam system can be operated at acceleration voltages up to 100 kV and is based on a 100 μm diameter flat single-crystal LaB_6 cathode with a capacity of delivering up to 2.4 mA of current. Using magnetic focusing lenses and alignment coils, the electrons are focused onto the liquid jet, generating a circular x-ray spot of FWHM down to 7 μm. X-rays are extracted at right angles to both the e-beam and the metal jet through a 127 μm thick Be output window, that separates the vacuum of the x-ray tube from atmospheric pressure.

III. RESULTS AND DISCUSSION

The spatial distribution of the source was characterized using an imaging arrangement consisting of a zone plate and an x-ray detector, as shown in Fig. 1. The zone plate is a gold plated, 75-μm diameter diffractive optic with an outermost zone width of 100 nm. As the focal length of the zone plate is energy dependent, the arrangement acts as a linear monochromator enabling energy-selective imaging of the source. Since the efficiency of the zone plate decreases rapidly for higher energies, the 9.25 keV Ga K_α peak was chosen for the imaging of the source. For this energy the zone plate has a first-order diffractive focal length of 5.75 cm. The x-ray detector is a 36 × 24 mm^2, 4008 × 2671 pixel fiber-coupled water-cooled CCD detector with a 15 μm thick, 5 mg/cm^2 Gd_2O_2S:Tb scintillator and 9 × 9 μm^2 pixels (Photonic Science). The FWHM of the point-spread function is 22 μm, which was determined from edge-spread-function measurements. This arrangement was used to form an 18 times magnified image of the source onto the detector. Throughout this process, the system was operated at 40 W with 50 kV acceleration voltage, and a 7 × 7 μm^2 FWHM x-ray spot was obtained, as shown in Fig. 1.

The quantitative spectral characterization of the source was performed using a CdTe-diode spectrometer (Amptek X-123CdTe). The spectral brightness was obtained from the CdTe-diode measurements and the measured source size. Figure 2 presents calibrated x-ray spectra, unfiltered and with 200 μm Al filtering, recorded at 30 W (50 kV, 0.6 mA). Al filtering decreases the low-energy emission that is highly absorbed in thick samples and is therefore used to reduce sample dose in the two imaging examples described below. By subtracting the bremsstrahlung, taking the natural line width (∼10.6 eV) of the doublet In K_α line[10] into account and assuming a 0.5 ratio[11] between $K_{\alpha1}$ and $K_{\alpha2}$, the peak spectral brightness was estimated to 3 × 10^9 photons/(s × mm^2 × mrad^2 × 0.1%BW).

The power loading capacity of the system, which limits the spectral brightness, is defined as the maximum attainable power loading of the e-beam when it hits the jet surface (expressed in W/μm). The current factor limiting the power loading is metal vapor from the jet anode causing cathode damage, as stated above. By defocusing the e-beam, the total e-beam power can be increased without generating debris. To determine the power loading capability, the location of the interaction point between e-beam and jet was chosen so that

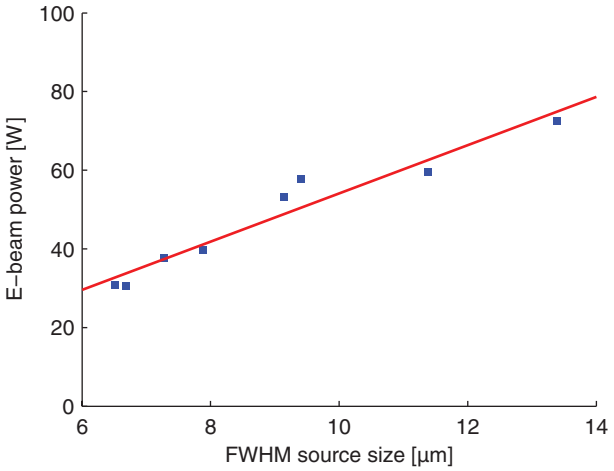

FIG. 3. (Color online) Power loading limit as a function of x-ray spot size.

the metal debris formation was maximized. For a given x-ray spot size, the e-beam power was increased until metal vapor was seen to affect the cathode. Figure 3 shows the power loading limit of the source as function of source size, as well as a least-square-fitted line. For example, for a circular 13 μm FWHM x-ray spot, the source power can be increased to 70 W. However, during normal operation the interaction point of the jet and e-beam is shifted so that the electrons hit the jet surface at a 45° angle, decreasing the amount of vapor that reaches the cathode. Thus, the power loading limit in Fig. 3 is conservative and the practical limit, especially for short experiments, is higher. For the imaging applications shown in Figs. 4 and 5, the source was operated at 40 W with a circular 7 μm x-ray spot giving an e-beam power density of around 1000 kW/mm^2. This corresponds to a power loading of 5.7 W/μm, which is roughly 7 times higher than that of solid stationary-anode microfocus sources.[2]

Finally, we note that the yield of the 24.2 keV line emission will depend on the choice of acceleration voltage. While increasing the acceleration voltage, e.g., from 50 kV to 100 kV will increase the line emission yield, it will also increase the amount of high-energy bremsstrahlung. Due to the low detection efficiency of our present detector at higher energies most of these photons will not be absorbed in the detector and, thus, only increase the dose delivered to the sample. For the biomedical applications discussed below it is vital that the sample radiation dose is small. The acceleration voltage was therefore chosen with equal weight to dose and exposure time. From simulations, the optimal acceleration voltage for the imaging applications in Figs. 4 and 5 is between 40 and 50 kV. An acceleration voltage of 50 kV was finally chosen since it allows tighter e-beam focusing and a higher e-beam power loading capability, resulting from increased electron penetration depth into the jet material.

IV. TOWARDS BIOMEDICAL IMAGING

To demonstrate the potential of the source for biomedical applications, a mammography phantom and an angiography phantom were separately imaged in an in-line phase-contrast arrangement.[12] This is a propagation-based technique where the phase contrast is created by refraction of x-rays by the sample. By moving the detector away from the sample, phase differences induced by the sample develop into intensity differences on the detector, which increases

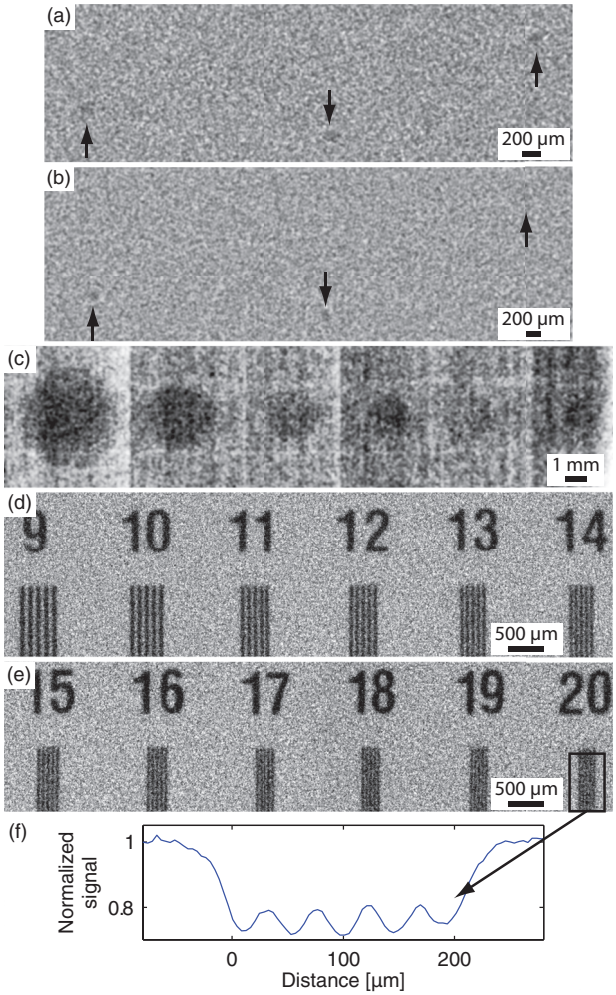

FIG. 4. (Color online) High-resolution x-ray imaging of a mammography phantom: (a) 165 μm diameter microcalcifications, (b) 130 μm microcalcifications, (c) tumor masses ranging from 4.76 mm down to 1.19 mm in diameter, (d) and (e) line pair targets, and (f) a line profile showing the signal for the 20 lp/mm line-pair target.

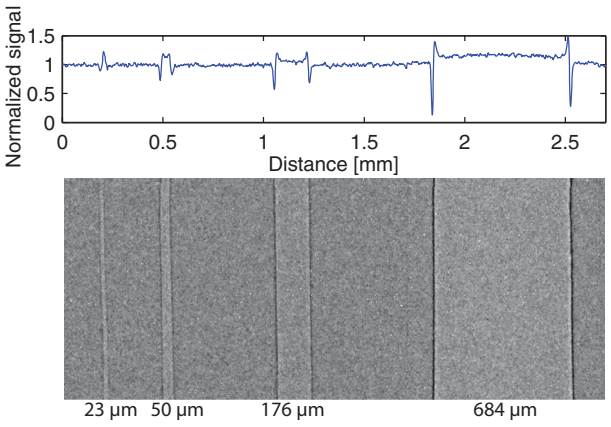

FIG. 5. (Color online) X-ray image and line profile of a phase-contrast angiography phantom consisting of gas-filled polyethylene tubes in water.

the signal from interfaces between materials, so-called edge-enhancement.

The mammography phantom (Model 11A, Computerized Imaging Reference Systems, Inc.) is made of 3.5 cm thick epoxy and contains, among other objects, microcalcifications ($CaCO_3$), hemispheric tumor masses, and line pair targets. Figure 4 shows images of the phantom using a 200 μm thick Al-hardened spectrum (cf. Fig. 2). The source-to-object and the object-to-detector distance were both 1.45 m, resulting in detectable phase-contrast contribution to the image, in addition to absorption effects. The exposure time was 180 s and the absorbed dose 4 mGy. This is slightly higher than the present limit (3 mGy) for mammography in the United States.[13] The dose is increased to compensate for the low efficiency of our present x-ray detector. Its quantum efficiency is 11% at 24 keV, while commercial mammography systems reach up to 60% efficiency.[14] Figures 4(a) and 4(b) show smoothed images of microcalcifications with diameters of 165 μm and 130 μm, respectively. Figure 4(c) has been binned and smoothed and shows tumor masses with diameters ranging from 4.76 mm down to 1.19 mm. In Fig. 4(e) all line pairs are visible, demonstrating a resolution better than 20 lp/mm inside 3.5 cm thick tissue. For clarity, a line profile taken across the 20 lp/mm target which has been averaged over the lines' full length is shown in Fig. 4(f). This suggests that the spatial resolution is high enough to resolve smaller microcalcifications if the detector efficiency could be increased to give sufficient signal-to-noise ratio in the image.

Figure 5 shows a phase-contrast image of the micro-angiography phantom, designed to mimic CO_2-filled blood vessels in mice.[15,16] The phantom consists of air-filled polyethylene tubes of thicknesses varying from 684 μm down to 23 μm, a range which corresponds to typical murine blood vessels. The polyethylene tubes are surrounded by 2 cm of water and two 140 μm thick glass windows which lead to a total x-ray absorption similar to that for 2 cm of soft tissue. For the experiment, the source was again filtered by 200 μm thick Al and the source-to-object and object-to-detector distances were 0.97 m and 1.93 m, respectively. The exposure time was 131 s and the dose 100 mGy, a typical dose in small-animal imaging.[17] As Fig. 5 shows, we can resolve the 23 μm diameter tubes in the water, suggesting potential for imaging blood vessels inside 2 cm thick tissue. Figure 5 also contains a line profile of the signal, integrated over 200 pixels in the vertical direction, which demonstrates the characteristic bright and dark fringes that constitutes the edge-enhancement of in-line phase contrast.

The higher photon energy and strong line emission of the source is relevant also in many x-ray scattering experiments[18] where higher penetrating power is needed because of sample surroundings such as reaction chambers, furnaces and high-pressure environments. Such XRD, SAXS, or WAXS (x-ray diffraction, and small- and wide-angle x-ray scattering) experiments can provide nanoscale structural and dynamical information on important biological and chemical substances and processes, and also have, for example, a potential diagnostic value for breast cancer.[19] Due to the low scattering efficiency of higher energy photons, these experiments are presently typically performed at synchrotron radiation facilities, making the high-brightness 24 keV liquid-metal-jet source demonstrated here potentially attractive for laboratory x-ray scattering experiments.[8]

Laboratory in-line phase-contrast imaging with low dose, requires both high-brightness sources and good x-ray detectors. High-brightness sources are needed to shorten the exposure times, which is essential to avoid motion blur. The detectors must have sufficiently high resolution to resolve the phase-contrast fringes, and high quantum efficiency. New and efficient high-resolution detectors are emerging,[20] with twice the efficiency of our present detector. A detector upgrade could therefore decrease the exposure time and thereby the dose by a factor of two while maintaining the same signal-to-noise ratio in the image. Increasing the power of microfocus sources is generally hard but fortunately the liquid-metal-jet-anode sources do not suffer from the same thermal limitations as conventional microfocus tubes. Instead cathode damage from metal vapor debris presently limits the power loading of the system. Among potential improvement strategies, shielding the cathode from metal vapor exposure by bending the electron-gun column[21] is a strong candidate. Still, a significant increase of the source power is required for many applications. For example, the exposure time of a typical mammography examination is less than 2 s per image,[22] making it necessary to increase source power by 1–2 orders of magnitude compared to the present arrangement. If feasible, however, such phase-contrast images (cf. Fig. 4) would have higher resolution and contrast than ordinary absorption images without any dose increase.

V. CONCLUSION

In summary, we have described a high-brightness 24 keV In K_α liquid-metal-jet-anode x-ray source. By changing the alloy of the original source platform and providing an experimental arrangement that supports operation at elevated temperatures, we were able to increase the In content from 21.5% to 65% and the 24-keV In K_α line yield by a factor of 3 or 4. The higher energy and increased line emission are beneficial in applications which require penetration through thicker objects or benefit from monochromatization. We have demonstrated the potential applicability of the source in the biomedical field by high-resolution imaging of a mammography phantom and a phase-contrast angiography phantom.

ACKNOWLEDGMENTS

This work has been supported by the Swedish Science Research Council and the Swedish Governmental Agency for Innovation Systems. The authors thank O. Hemberg, M. Otendal, and T. Tuohimaa of Excillum AB, and E. Fredenberg and M. Åslund of Philips Women's Healthcare for valuable discussions.

[1]O. Hemberg, M. Otendal, and H. M. Hertz, Appl. Phys. Lett. **83**, 1483 (2003).
[2]M. Otendal, T. Tuohimaa, U. Vogt, and H. M. Hertz, Rev. Sci. Instrum. **79**, 016102 (2008).
[3]E. Krestel, *Imaging Systems for Medical Diagnostics* (Siemens, Berlin, 1990).

[4]D. E. Grider, A. Wright, and P. K. Ausburn, J. Phys. D **19**, 2281 (1986).
[5]O. Hemberg, M. Otendal, and H. M. Hertz, Opt. Eng. **43**, 1682 (2004).
[6]M. Otendal, T. Tuohimaa, O. Hemberg, and H. M. Hertz, in *X-Ray Sources and Optics*, SPIE Int. Soc. Opt. Eng., Bellingham, 2004, Vol. 5537, edited by C. A. MacDonald, A. T. Macrander, T. Ishikawa, C. Morawe, and J. L. Wood (Denver, Colorado, 2004), p. 57.
[7]I. Szaloki, J. Osan, and R. E. Van Grieken, Anal. Chem. **78**, 4069 (2006).
[8]R. Gorgl and G. Maier, J. Phys. IV **118**, 53 (2004).
[9]T. Tuohimaa, M. Otendal, and H. M. Hertz, Appl. Phys. Lett. **91**, 074104 (2007).
[10]M. O. Krause, J. Phys. Chem. Ref. Data **8**, 307 (1979).
[11]M. C. Martins, M. I. Marques, F. Parente, and J. G. Ferreira, J. Phys. B **22**, 3167 (1989).
[12]S. C. Mayo, P. R. Miller, S. W. Wilkins, T. J. Davis, D. Gao, T. E. Gureyev, D. Paganin, D. J. Parry, A. Pogany, and A. W. Stevenson, J. Microsc. **207**, 79 (2002).
[13]Mammography Quality Standards Act, CFR §21, 900.12 (1995).
[14]P. Monnin, D. Gutierrez, S. Bulling, D. Guntern, and F. R. Verdun, Med. Phys. **34**, 906 (2007).
[15]A. Burvall, U. Lundström, P. A. C. Takman, D. H. Larsson, and H. M. Hertz, Opt. Express **19**, 10359 (2011).
[16]U. Lundström, D. H. Larsson, A. Burvall, P. A. C. Takman, L. Scott, H. Brismar, and H. M. Hertz, "X-ray phase contrast for CO_2 microangiography," Phys. Med. Biol. (submitted).
[17]F. Kiessling, S. Greschus, M. P. Lichy, M. Bock, C. Fink, S. Vosseler, J. Moll, M. M. Mueller, N. E. Fusenig, H. Traupe, and W. Semmler, Nat. Med. **10**, 1133 (2004).
[18]B. D. Cullity and S. R. Stock, *Elements of X-ray Diffraction*, 3rd International ed. (Prentice Hall, Upper Saddle River, New Jersey, 2001).
[19]M. Fernandez, J. Keyrilainen, R. Serimaa, M. Torkkeli, M. L. Karjalainen-Lindsberg, M. Tenhunen, W. Thomlinson, V. Urban, and P. Suortti, Phys. Med. Biol. **47**, 577 (2002).
[20]O. Svenonius, A. Sahlholm, P. Wiklund, and J. Linnros, Nucl. Instrum. Methods Phys. Res. A **607**, 138 (2009).
[21]Y. Arata and M. Tomie, Trans. JWRI **9**, 157 (1980).
[22]C. Honda, H. Ohara, and T. Gido, in *Digital Mammography, Proceedings, Manchester, UK, 2006*, edited by S. M. Astley, M. Brady, C. Rose, and R. Zwiggelaar (Springer-Verlag, Berlin, 2006), Vol. 4046, p. 281.